# Boiling Quantum Vacuum: Thermal Subsystems from Ground-State Entanglement

Ali G. Moghaddam[1,2] Kim Pöyhönen[1,2] and Teemu Ojanen[1,2,*]

[1] *Computational Physics Laboratory, Physics Unit, Faculty of Engineering and Natural Sciences, Tampere University, Tampere FI-33014, Finland*

[2] *Helsinki Institute of Physics, University of Helsinki FI-00014, Finland*

(Received 5 April 2022; revised 9 August 2022; accepted 16 August 2022; published 8 September 2022)

In certain special circumstances, such as in the vicinity of a black hole or in a uniformly accelerating frame, vacuum fluctuations appear to give rise to a finite-temperature environment. This effect, currently without experimental confirmation, can be interpreted as a manifestation of quantum entanglement after tracing out vacuum modes in an unobserved region. In this work, we identify a class of experimentally accessible quantum systems where thermal density matrices emerge from vacuum entanglement. We show that reduced density matrices of lower-dimensional subsystems embedded in $D$-dimensional gapped Dirac fermion vacuum, either on a lattice or continuum, have a thermal form with respect to a lower-dimensional Dirac Hamiltonian. Strikingly, we show that vacuum entanglement can even conspire to make a subsystem of a gapped system at zero temperature appear as a hot gapless system. We propose concrete experiments in cold-atom quantum simulators to observe the vacuum-entanglement-induced thermal states.

DOI: 10.1103/PRXQuantum.3.030335

## I. INTRODUCTION

Thermalization is one of the most widespread and fundamental phenomena and plays a central role in virtually all branches of physics. In standard textbook statistical physics, a thermal state arises as a maximum entropy state that satisfies appropriate external constraints [1]. More recently, the notion of the eigenstate thermalization hypothesis has identified temperature as a generic emergent phenomenon in closed quantum systems [2–4]. According to the hypothesis, the reduced density matrix of a subsystem of a thermodynamically large, interacting many-body system is asymptotically equal to the thermal reduced density matrix when the subsystem is sufficiently small compared to the total system [5–7]. This hypothesis in its strong form, where all eigenstates become thermalized, has been verified for nonintegrable systems [8]. A weaker version, such that an exponentially small number of nonthermal states can exist, has been observed in certain integrable models as well [9].

While the eigenstate thermalization hypothesis only accounts for a nonzero temperature in highly excited systems, there are famous examples of how vacuum fluctuations may give rise to a finite-temperature environment. The Hawking effect, which attributes a finite temperature to black holes, is deeply connected to the entanglement of vacuum modes [10–12]. In the same vein, the Unruh effect gives rise to a finite temperature for accelerated observers moving in the relativistic vacuum. In both cases, the apparent unitarity-violating emergence of a thermal state could be attributed to entanglement with an unobservable region beyond the event horizon or the Rindler wedge. It has been recognized that this picture is valid in a much broader sense, promoting entanglement as the key unifying concept in analyzing diverse phenomena from black hole physics to condensed-matter systems [13–22]. For example, the emergence of effective temperature from ground-state entanglement has lately been identified in systems obeying the entanglement *area law*, where the entanglement entropy scales as the subsystem boundary [22–24]. The area law is known to give rise to subsystem density matrices that are characterized by a spatially varying effective temperature that decreases rapidly away from the boundaries [25–29]. Unfortunately, the strongly inhomogeneous entanglement temperature profile is mostly of theoretical interest since its experimental verification poses so far unresolved practical and conceptual issues. However, a direct experimental observation of a thermal state emerging from vacuum entanglement would be an outstanding achievement with deep implications for multiple branches of physics.

*Email: teemu.ojanen@tuni.fi

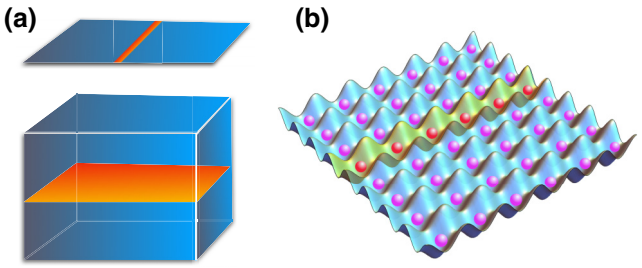


FIG. 1. Entanglement-induced thermal subsystems embedded in a $D$-dimensional Dirac fermion system at zero temperature. (a) Examples of lower-dimensional thermal subsystems embedded in 2D and 3D parent states. When the full system is in the ground state of the total system Hamiltonian $\mathcal{H}_D$, the reduced density matrix of the subsystem has a thermal form $\rho = e^{-\beta\mathcal{H}_{D-1}}/\mathcal{Z}$. (b) Thermal state emerging from vacuum entanglement could be observed in cold-atom quantum simulators by probing particle fluctuations in the one-dimensional subsystem.

In this work, we identify a large class of systems, illustrated in Fig. 1(a), where vacuum entanglement induces a uniform temperature and where the phenomenon becomes experimentally accessible. Specifically, we show that the lower-dimensional subsystems embedded in a $D$-dimensional gapped Dirac fermion vacuum have thermal density matrices. This property holds for continuum models as well as for lattice systems. The thermal Hamiltonian of a subsystem has a simple relation to the Hamiltonian of the whole system, while the effective temperature is determined by the bandwidth in the traced-out directions. For lattice systems, the effective temperature acquires momentum dependence; however, typically, the density matrix is excellently reproduced by a constant-temperature approximation. We explain how the notion of lower-dimensional thermal subsystems is closely connected to the table of topological insulators in different dimensions. As a striking consequence of our results, we show that the vacuum entanglement can conspire to make lower-dimensional subsystems of a zero-temperature gapped state appear as hot gapless systems. Finally, we explain how the thermal nature of the subsystems manifests through fluctuations in observables and propose a concrete setup, illustrated in Fig. 1(b), where our predictions can be verified in cold-atom quantum simulators. Specifically, we show that the particle number fluctuations in a one-dimensional (1D) chain embedded in a 2D array match those of a genuinely 1D Dirac system at finite temperature, providing a smoking gun signature of the vacuum-entanglement-induced thermal state.

## II. THERMAL ENTANGLEMENT SPECTRA IN $D$-DIMENSIONAL GAPPED FERMI SYSTEMS

In this section, we study lower-dimensional subsystems embedded in the ground state of a gapped $D$-dimensional Dirac fermion system with the Hamiltonian

$$H_D(\mathbf{k}) = \sum_\mu d_{D\mu}(\mathbf{k})\Gamma^\mu \equiv \mathbf{d}_D(\mathbf{k})\cdot\mathbf{\Gamma}, \tag{1}$$

where $\Gamma^\mu$ are $2^n$-dimensional (with $n \in \mathbb{N}$) Clifford matrices $\{\Gamma^\mu, \Gamma^\nu\} = 2\mathbb{1}\delta^{\mu\nu}$ and $\mathbf{d}_D$ satisfies $\mathbf{d}_D \cdot \mathbf{d}_D > 0$ for all $D$-dimensional (quasi)momenta $\mathbf{k} \in \mathbb{R}^D$. In particular, we show that the reduced density matrix of a $D_s$-dimensional translation-invariant subsystem ($D_s < D$) can be exactly written in the form

$$\rho_{D_s} = \frac{e^{-\sum_{k_s}\beta(\mathbf{k}_s)\hat{d}^\dagger_{\mathbf{k}_s}H_{D_s}(\mathbf{k}_s)\hat{d}_{\mathbf{k}_s}}}{\mathcal{Z}}, \tag{2}$$

where the effective subsystem Hamiltonian (ESH) $H_{D_s}(\mathbf{k}_s) = \mathbf{d}_{D_s}(\mathbf{k}_s)\cdot\mathbf{\Gamma}$ has a Dirac form with a lower-dimensional momentum $\mathbf{k}_s \in \mathbb{R}^{D_s}$ and the $\hat{d}_{\mathbf{k}_s}$ are fermion annihilation operators. The reduced density matrix in Eq. (2) in its general form corresponds to a *generalized Gibbs ensemble* that reduces to an exactly thermal density matrix for a constant $\beta$ [30]. We obtain an analytical expression for the effective translation-invariant inverse temperature $\beta(\mathbf{k}_s)$ and demonstrate with examples how expression (2) typically holds to remarkable accuracy when $\beta(\mathbf{k}_s)$ is approximated by a constant. Despite the system as a whole being in the quantum ground state, from the point of view of observables, the subsystems behave as $D_s$-dimensional systems at finite temperature. We note that the ESH should not be confused with the commonly studied entanglement Hamiltonian $H_E$, defined by $\rho_{D_s} = e^{-H_E}/\mathcal{Z}$. In contrast to the ESH, the entanglement Hamiltonian does not provide a natural notion of temperature, and it does not reduce to the subsystem Hamiltonian even when all couplings between the reduced subsystem and the rest vanish.

### A. Entanglement-temperature mapping

Here we derive the entanglement-temperature mapping in Eq. (2). For a free-fermion system in a Gaussian state, including (but not limited to) the ground state and a finite-temperature state, the reduced density matrix of an arbitrary subsystem also corresponds to a Gaussian state [31,32]. Consequently, due to Wick's theorem, the entanglement spectrum of a subsystem is completely encoded in the correlation matrix with real-space components defined as $\mathcal{C}^{\alpha\alpha'}_{\mathbf{x},\mathbf{x}'} = \langle\hat{c}^\dagger_{\mathbf{x}\alpha}\hat{c}_{\mathbf{x}'\alpha'}\rangle^*$ given in terms of fermion operators $\hat{c}_{\mathbf{x}\alpha}$ for a particle with orbital index $\alpha$ and at position $\mathbf{x}$ in the subsystem. If two systems have the same correlation matrices, they necessarily have coinciding reduced density matrices. Here, by matching the correlation matrices, we map the reduced density matrix of $D_s$-dimensional subsystems to thermal $D_s$-dimensional systems given by Eq. (2). In translationally invariant systems, by expanding

particle creation operators in the basis of Bloch eigenstates $\psi_{\nu\mathbf{k}}$ as $\hat{c}^\dagger_{\mathbf{k}\alpha} = \sum_\nu \langle\alpha|\psi_{\nu\mathbf{k}}\rangle \hat{d}^\dagger_{\nu\mathbf{k}}$ we find the correlation matrix elements in $k$ space as

$$\langle \hat{c}^\dagger_{\mathbf{k}\alpha}\hat{c}_{\mathbf{k}\alpha'}\rangle^* = \sum_\nu \langle\alpha|\psi_{\nu\mathbf{k}}\rangle\langle\psi_{\nu\mathbf{k}}|\alpha'\rangle\langle \hat{d}^\dagger_{\nu\mathbf{k}}\hat{d}_{\nu\mathbf{k}}\rangle,$$

where the expectation value on the right-hand side gives the Fermi-Dirac distribution $n_F(E_{\nu\mathbf{k}})$. In the following, we assume that the parent $D$-dimensional system is at zero temperature so $n_F(E_{\nu\mathbf{k}})$ is 1 for filled bands and 0 for others. It is now straightforward to show that, by restricting spatial indices $\mathbf{x}, \mathbf{x}'$ to a $D_s$-dimensional subsystem with periodic boundary conditions, the correlation matrix becomes

$$\begin{aligned} \mathcal{C}^{\alpha\alpha'}_{\mathbf{x},\mathbf{x}'} &= \frac{1}{L^D}\sum_{\mathbf{k}} e^{-i\mathbf{k}\cdot(\mathbf{x}-\mathbf{x}')}\langle \hat{c}^\dagger_{\mathbf{k}\alpha}\hat{c}_{\mathbf{k}\alpha'}\rangle^* \\ &= \frac{1}{L^{D_s}}\sum_{\mathbf{k}_s} e^{-i\mathbf{k}_s\cdot(\mathbf{x}-\mathbf{x}')}\langle\alpha|\hat{\mathcal{C}}^{\text{sub}}(\mathbf{k}_s)|\alpha'\rangle, \end{aligned} \tag{3}$$

where $L$ is the linear extent of the system in all $D$ dimensions and

$$\hat{\mathcal{C}}^{\text{sub}}(\mathbf{k}_s) = \frac{1}{L^{D-D_s}}\sum_{\text{filled }\nu,\mathbf{k}_\perp} |\psi_{\nu\mathbf{k}}\rangle\langle\psi_{\nu\mathbf{k}}|. \tag{4}$$

This defines the Fourier transform of the subsystem correlation matrix that has been obtained simply by substituting the above expression for $\langle \hat{c}^\dagger_{\mathbf{k}\alpha}\hat{c}_{\mathbf{k}\alpha'}\rangle^*$. The full $D$-dimensional momentum $\mathbf{k} = (\mathbf{k}_s, \mathbf{k}_\perp)$ is decomposed as the reduced subsystem momentum $\mathbf{k}_s$ with $D_s$ components, and the momentum perpendicular to subsystem $\mathbf{k}_\perp$ with $D - D_s$ components. We note that, since the Hamiltonian is expressed in terms of anticommuting gamma matrices, the number of different orbitals (bands) $\alpha$ is also limited to $2^n$ and the correlation matrix $\hat{\mathcal{C}}$ must be $2^n \times 2^n$, accordingly. The entanglement spectrum and the reduced density matrix are now fully determined by the correlation matrix (3).

The correlation matrix of a genuinely $D_s$-dimensional system at a finite temperature is also given by expression (3) but now with operator $\hat{\mathcal{C}}^{\text{sub}}(\mathbf{k}_s)$ substituted by

$$\hat{\mathcal{C}}^{\text{th}}(\mathbf{k}_s) = \sum_\nu |\phi_{\nu\mathbf{k}_s}\rangle\langle\phi_{\nu\mathbf{k}_s}| n_F(\omega_{\nu\mathbf{k}_s}), \tag{5}$$

where $|\phi_{\nu\mathbf{k}_s}\rangle$ and $\omega_{\nu\mathbf{k}}$ are eigenstates and energies of a $D_s$-dimensional Hamiltonian. The necessary and sufficient condition for the thermal mapping of the reduced density matrix of $D_s$-dimensional subsystems is that expressions (4) and (5) must match for some $D_s$-dimensional Hamiltonian $H_{D_s}$. Thus, the emergence of an effective temperature in the reduced density matrix of the subsystem arises from the momentum average of $D$-dimensional band projectors over the $D - D_s$ unobserved dimensions. Equations (3)–(5) are valid for all free-fermion systems.

We now show how the generalized Dirac systems (1) provide a natural example of the entanglement-temperature correspondence in Eq. (2). The spectrum of the $D$-dimensional parent Hamiltonian (1) is given by $\varepsilon_{\mathbf{k}} = \pm|\mathbf{d}_D(\mathbf{k})|$ and the projection to the filled negative-energy bands is obtained by

$$\sum_{\text{filled }\nu} |\psi_{\nu\mathbf{k}}\rangle\langle\psi_{\nu\mathbf{k}}| = \frac{1}{2}\left(\mathbb{1} - \frac{\mathbf{d}_D}{|\mathbf{d}_D|}\cdot\boldsymbol{\Gamma}\right).$$

Hence, we find that

$$\hat{\mathcal{C}}^{\text{sub}}(\mathbf{k}_s) = \frac{1}{2}\left(\mathbb{1} - \left\langle\frac{\mathbf{d}_D}{|\mathbf{d}_D|}\right\rangle_\perp\cdot\boldsymbol{\Gamma}\right) \tag{6}$$

with

$$\langle\cdot\rangle_\perp = L^{-(D-D_s)}\sum_{\mathbf{k}_\perp}\cdot$$

denoting the momentum average over the traced-over dimensions. Defining a new quantity

$$\mathbf{d}_{D_s}(\mathbf{k}_s) = \frac{1}{\mathcal{F}_{D_s}(\mathbf{k}_s)}\left\langle\frac{\mathbf{d}_D}{|\mathbf{d}_D|}\right\rangle_\perp, \tag{7}$$

where

$$\mathcal{F}_{D_s}(\mathbf{k}_s) = \left\langle\frac{1}{|\mathbf{d}_D|}\right\rangle_\perp, \tag{8}$$

the correlation matrix (6) for the reduced system becomes

$$\hat{\mathcal{C}}^{\text{sub}}(\mathbf{k}_s) = \tfrac{1}{2}(\mathbb{1} - \mathcal{F}_{D_s}\mathbf{d}_{D_s}\cdot\boldsymbol{\Gamma}). \tag{9}$$

This is immediately similar to the thermal correlation matrix of a genuinely $D_s$-dimensional system with a Dirac Hamiltonian $H_{D_s} = \mathbf{d}_{D_s}(\mathbf{k}_s)\cdot\boldsymbol{\Gamma}$. Using Eq. (5), the thermal correlation matrix for such a system reads

$$\hat{\mathcal{C}}^{\text{th}}(\mathbf{k}_s) = \frac{1}{2}\sum_{\eta=\pm1}\left(\mathbb{1} + \eta\frac{\mathbf{d}_{D_s}}{|\mathbf{d}_{D_s}|}\cdot\boldsymbol{\Gamma}\right)n_F(\eta|\mathbf{d}_{\mathbf{k}_s}|),$$

which can be matched with Eq. (9) by requiring that

$$\mathcal{F}_{D_s}(\mathbf{k}_s) = \frac{n_F(-|\mathbf{d}_{D_s}|) - n_F(|\mathbf{d}_{D_s}|)}{|\mathbf{d}_{D_s}|}.$$

From this equation we can solve the effective entanglement temperature as

$$T(\mathbf{k}_s) = \beta^{-1}(\mathbf{k}_s) = \frac{|\mathbf{d}_{D_s}|}{2\,\text{arctanh}(|\mathbf{d}_{D_s}|\mathcal{F}_{D_s})}. \tag{10}$$

ESH (7) and temperature (10) fix the entanglement-temperature mapping in Eq. (2), proving that the ground-state entanglement in lower-dimensional subsystems gives rise to a thermal density matrix. This density matrix is characterized by a translation-invariant temperature and the ESH $H_{D_s}$ that is obtained by averaging the parent Hamiltonian $H_D$ over the unobserved directions. The entanglement temperature (10) is of the order of the bandwidth (or the hopping amplitude) in the traced-out dimensions and, as such, is very high for isotropic models. In strong contrast to generic area-law subsystems that exhibit a strongly inhomogeneous spatial temperature profile [27,28], the entanglement entropy here scales as the subsystem volume, and the effective temperature for lower-dimensional systems can be typically regarded as a constant, as seen below. The analogy to a true thermal equilibrium state with uniform temperature makes the phenomenon feasible to experimental studies.

### B. Example I: 1D thermal subsystems in a Chern insulator

To make the general entanglement-temperature mapping more concrete, we now illustrate it by examples. First we study a 2D Chern insulator model and show that its 1D subsystems correspond to thermal 1D systems. In particular, we consider the Qi-Wu-Zhang (QWZ) model defined by $H_{2D} = \mathbf{d}_{2D}(\mathbf{k}) \cdot \boldsymbol{\sigma}$ with $\mathbf{d}_{2D}(\mathbf{k}) = (t_x \sin k_x, t_y \sin k_y, m - t_x \cos k_x - t_y \cos k_y)$. For the sake of compactness, in the following we set $t_x = 1$, which is equivalent to measuring all other energy scales with respect to that quantity. The correlation matrix given by Eq. (4), for a 1D subsystem in x direction and with the valence band filled for the 2D model, reads

$$\begin{aligned}\mathcal{C}(k_x) &= \frac{1}{L}\sum_{k_y} |\psi_{\mathbf{k},-}\rangle\langle\psi_{\mathbf{k},-}| \\ &= \frac{1}{2}\left[\mathbb{1} - \frac{1}{L}\sum_{k_y} \frac{\mathbf{d}_{2D}(\mathbf{k})}{|\mathbf{d}_{2D}(\mathbf{k})|}\cdot\boldsymbol{\sigma}\right]\end{aligned}$$

with $|\psi_{\mathbf{k},-}\rangle$ indicating the negative-energy eigenstates. The averaging over vertical momentum, using the expression for the vector $\mathbf{d}_{2D}$, can be written as

$$\begin{aligned}\frac{1}{L}\sum_{ky} \frac{\mathbf{d}_{2D}(\mathbf{k})}{|\mathbf{d}_{2D}(\mathbf{k})|} &= (\sin k_x, 0, m - \cos k_x)\mathcal{F}(k_x) \\ &\quad - (0,0,1)\frac{1}{L}\sum_{ky} \frac{t_y \cos k_y}{|\mathbf{d}_{2D}(\mathbf{k})|},\end{aligned}$$

in which $\mathcal{F}(k_x) = (1/L)\sum_{k_y} 1/|\mathbf{d}_{2D}(\mathbf{k})|$. It is clear that the average of the second component of the vector identically vanishes due to its antisymmetry under $k_y \to -k_y$. The second line can also simply be absorbed inside the mass term $m$ as a renormalization,

$$\delta m(k_x) = \frac{1}{\mathcal{F}(k_x)}\frac{t_y}{L}\sum_{k_y} \frac{\cos k_y}{|\mathbf{d}_{2D}(\mathbf{k})|}.$$

Putting altogether, the correlation matrix of the 1D subsystem takes the form

$$\mathcal{C}(k_x) = \tfrac{1}{2}[\mathbb{1} - \mathcal{F}(k_x)\,\mathbf{d}_{1D}(k_x)\cdot\boldsymbol{\sigma}] \tag{11}$$

with

$$\mathbf{d}_{1D}(k_x) = [\sin k_x, 0, m - \delta m(k_x) - \cos k_x]. \tag{12}$$

The 1D ESH determining the thermal state is given by Eq. (12), which has the form of $H_{2D}$ with vanishing transverse hopping $t_y = 0$ and renormalized mass $m + \delta m(k_x)$. In other words, the 1D subsystem embedded in the 2D QWZ model has the same static properties as a vertically decoupled 1D chain with just a renormalized mass, and subjected to a temperature, as will be elucidated more clearly in the following. The dependence of the mass renormalization term $\delta m$ on momentum for different values of $m$ and $t_y$ is shown in Figs. 2(a) and 2(b), respectively. Intriguingly, the mass renormalization vanishes identically when $m = 1$ and $k_x = 0$, which can also be deduced from the mass renormalization expression by noting that at this particular point we have $\mathbf{d}_{2D}(k_x = 0, k_y) = t_y(0, \sin k_y, -\cos k_y)$, thereby $\delta m(k_x = 0)|_{m=1} = 0$. But, since $m = 1$ corresponds to the gap-closing point of the 1D model with $\tilde{\mathbf{d}}_{1D} = (\sin k_x, 0, m - \cos k_x)$, the above observation implies that the gap-closing point of the ESH given by Eq. (12) at $m = 1$ is not affected by $\delta m$. As shown in Appendix A, this behavior is not limited to the simple model with just nearest-neighbor hopping. We also see that $\delta m$ is suppressed by decreasing the lateral hopping and vanishes when $t_y \to 0$, as expected.

Result (11) can be recast into a manifestly thermal form as

$$\mathcal{C}(k_x) = \frac{1}{2}\sum_{\eta=\pm1}\left(\mathbb{1} + \eta\frac{\mathbf{d}_{1D}}{|\mathbf{d}_{1D}|}\cdot\boldsymbol{\sigma}\right)n_F(\eta|\mathbf{d}_{1D}|),$$

where the temperature is obtained from Eq. (10) as

$$T(k_x) = \frac{|\mathbf{d}_{1D}|}{2\,\mathrm{arctanh}(|\mathbf{d}_{1D}|\mathcal{F})}.$$

This temperature is plotted in Fig. 2(c) for various values of the mass $m$ and in Fig. 2(d) for different values of the transverse hopping $t_y$. As seen in Fig. 2(d), the scale of the temperature is set by the transverse hopping $t_y$, as expected. The temperature has a weak dependence

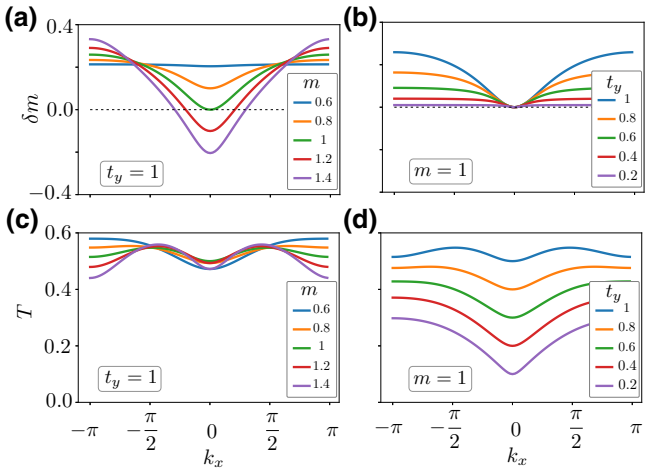


FIG. 2. Entanglement temperature and mass renormalization in the QWZ model. Panels (a) and (b) show the dependence of the mass renormalization $\delta m$ on the momentum $k_x$ for different values of $m$ and $t_y$, respectively. As discussed in the text, $\delta m$ identically vanishes at the gap-closing point when $m = 1$ and $k_x = 0$. Panels (c) and (d) show the variation of the effective temperature with momentum.

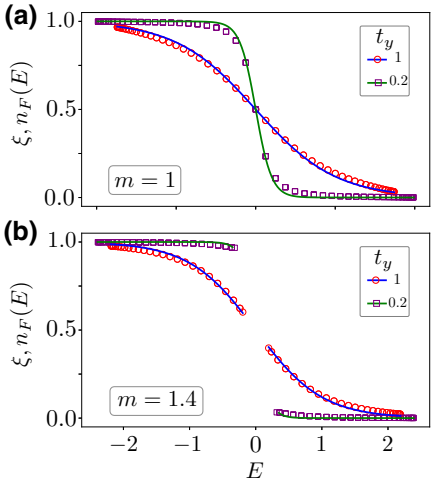


FIG. 3. Thermal population of a 1D subsystem in the QWZ model. (a) Correlation matrix spectra for the 1D subsystem (shown by circles and squares) and a thermal system (shown by lines) for $m = 1$ and two different values of lateral hopping. (b) Similar results for $m = 1.4$. In both panels, the thermal correlation spectrum is given by the Fermi-Dirac distribution $n_F(E)$ at temperatures $T = 0.5$ (for $t_y = 1$) and $T = 0.1$ (for $t_y = 0.2$), and plotted as a function of the ESH energy $E = \pm|\mathbf{d}_{1D}(k_x)|$.

on momentum, especially around $m \sim 1$ where the gap of the effective 1D model (12) closes. Now, remembering that at $m = 1$ the parent 2D system is gapped, this has an interesting consequence that the reduced density matrix of a 1D subsystem for $m = 1$ matches that of a *gapless* system at a very high temperature, even though we started from a gapped 2D system in its ground state. This result stems from the fact that, as we have noted earlier, the ESH is equivalent to decoupled 1D chains accompanied with a mass renormalization that itself vanishes at the gap-closing point of the decoupled chains. Moreover, as we will see in the next section, a similar behavior is also revealed in higher dimensions, which makes this result quite profound, especially noting that the inclusion of further hopping terms may result in the same final result (Appendix A). In Sec. III, we elaborate more on the physical reasons behind the appearance of gapless subsystems of gapped systems, in a broader sense.

Thermalization is further confirmed in Fig. 3, which shows a comparison between the exact correlation matrix eigenvalues (denoted by $\xi$) and the corresponding thermal model with constant temperature. The correlation matrix eigenvalues provide the occupation probabilities of the subsystem states and are given by the Fermi-Dirac distribution at finite temperature. As seen in Fig. 3(a), the constant temperature Fermi-Dirac distribution essentially reproduces the exact results. Away from $|m| = 1$, ESH (12) is gapped, as indicated by the correlation matrix spectrum in Fig. 3(b). In Sec. IV we discuss how the entanglement-induced thermal state and the gapless subsystems can be observed through experimentally measurable fluctuations.

### C. Example II: Dirac models with linear dispersion

We now show that the entanglement-temperature mapping of lower-dimensional subsystems becomes simple for continuum Dirac models with linear dispersion in arbitrary spatial dimensions. For simplicity, we consider the two-dimensional case, but generalization to higher dimensions is straightforward. Let us consider Hamiltonian $H_{2D} = \mathbf{d}_{2D}(\mathbf{k}) \cdot \boldsymbol{\sigma}$ with $\mathbf{d}_{2D}(\mathbf{k}) = (k_x, k_y, m)$ representing a 2D massive Dirac Hamiltonian. Adapting Eqs. (7) and (8) derived for lattice systems to continuum, we obtain the effective 1D Hamiltonian of the corresponding thermal system as $\mathbf{d}_{1D}(\mathbf{k}) = (k_x, 0, m)$ and

$$\mathcal{F} = \frac{1}{2\Lambda}\int_{-\Lambda}^{\Lambda} \frac{dk_y}{\sqrt{k_x^2 + k_y^2 + m^2}} \approx \frac{1}{2\Lambda} \ln\left(\frac{4\Lambda^2}{k_x^2 + m^2}\right).$$

Here, a finite high-energy cutoff $\Lambda$ is required to avoid logarithmic divergence of the integral, and the final result is justified by assuming that $\Lambda \gg \sqrt{k_x^2 + m^2}$. According to Eq. (10), the effective temperature reads

$$T = \frac{\Lambda}{2\ln(2\Lambda/\sqrt{k_x^2 + m^2})} \approx \frac{\Lambda}{2\ln(2\Lambda/m)}, \qquad (13)$$

which means that it is only weakly dependent on momentum and becomes constant in the small-momentum limit $k_x \ll m \ll \Lambda$. Similarly, for higher dimensions, the effective $D_s$-dimensional Hamiltonian determining the reduced density matrix in Eq. (2) is given by $H_D(\mathbf{k}_s)$ and the scale

of the effective temperature is set by the cutoff scale $\Lambda$. Result (13) shows that, for the temperature mapping to apply at small momentum, it is necessary to have a finite mass $|m| > 0$ to avoid infrared divergences.

### D. ESH versus the Bisognano-Wichmann Hamiltonian

Above we noted the difference between the entanglement Hamiltonian and the ESH for lower-dimensional subsystems. Here we emphasize that the entanglement temperature and the ESH found in our work neither follow nor are consistent with the well-known Bisognano-Wichmann (BW) theorem that has enjoyed renewed interest recently. This theorem states that the entanglement Hamiltonian for a half-partitioning of Lorentz-invariant systems exactly follows the system Hamiltonian with just an additional spatially varying prefactor besides the local Hamiltonian density of the original system [25,27]. The first obvious difference is that, unlike the BW Hamiltonian, the ESH need not contain any position dependence since our subsystems are of lower dimension and are (lattice) translation invariant themselves. The second and even more important difference is that the ESH does not follow the system Hamiltonian as we have seen explicitly for prototype examples. In fact, the ESH can have a completely different spectrum and physical behaviour from the original Hamiltonian. This is reflected in the surprising physical effect that the reduced density matrices of lower-dimensional subsystems of a gapped parent system can mimic that of a gapless system. Moreover, our thermal mapping is mathematically exact, and we find a renormalization of the Hamiltonian parameters—for instance, the mass parameter $m$ of Dirac models—in the ESH, which is not consistent with the BW form of the entanglement Hamiltonian.

On top of the above distinctions, the temperature associated with the ESH and the renormalization of the parameters is controllable by adjusting the lateral hopping strength, as seen above. This possibility to physically disentangle the notion of temperature and the ESH is absent in the BW framework since, relying just on the standard notion of the entanglement Hamiltonian and BW form, we always suffer from indistinguishable dual interpretations: (a) a uniform Hamiltonian accompanied by spatially varying effective temperature, (b) a spatially varying BW Hamiltonian and a constant effective temperature. Not to mention that we can have even further mathematically valid choices between the two above limiting interpretations.

Even if one attempted to settle the ambiguity of disentangling physically relevant temperature by simply regarding the BW form of the reduced density matrix in terms of a constant Hamiltonian and spatially varying temperature profile, one would run into serious practical problems when trying to experimentally confirm the temperature profile. To probe the reduced density matrix, one would need probe the reduced system as a whole. But, since the postulated effective entanglement temperature profile is strongly spatially dependent, one would also need to probe the reduced system locally to confirm the temperature profile. This leads to a dichotomy that one would simultaneously need to observe the whole system as well as probe its local properties. Thus, experimentally measuring any spatially varying temperature associated with the BW theorem is deeply problematic in ways that highlight its different nature with ordinary temperature profiles.

### E. Thermal subsystems from vacuum entanglement versus genuine thermal states

Since a density matrix encodes the full information of the state of a system at a given moment in time, all single-time expectation values and subsystem observables obtained from the density matrix (2) will coincide with those of a $D_s$-dimensional system with Hamiltonian $H_{D_s}$ at finite temperature. However, it is clear that the entanglement-induced effective thermal subsystems exhibit crucial departures from true thermal states. In general, thermal systems emit thermal radiation and perturb their environment by thermal fluctuations. Since the full $D$-dimensional system (1) is in the ground state, it is obviously impossible to extract net energy from any of its subsystems. Thus, contrary to naive expectations, the static thermal mapping (2) does not imply that lower-dimensional subsystems would inherit all the properties of thermal states.

To further quantify the above stated limitations, one can consider time-dependent generalization of the correlation operator (4), i.e.,

$$\hat{\mathcal{C}}^{\mathrm{sub}}(\mathbf{k}_s;t) = \frac{1}{L^{D-D_s}} \sum_{\text{filled } \nu,\mathbf{k}_\perp} e^{-iE_{\nu\mathbf{k}}t} |\psi_{\nu\mathbf{k}}\rangle\langle\psi_{\nu\mathbf{k}}|, \qquad (14)$$

which depends on the full energy spectrum (excitations) $E_{\nu\mathbf{k}}$ of the higher-dimensional parent system. Since the density matrix (2) contains only the ground-state information, it is insufficient in obtaining the time- and frequency-dependent correlations necessary to establish many standard properties of thermal systems, such as the fluctuation-dissipation theorem. At very short times compared to the inverse of the bandwidth ($t \ll 1/\Delta E$), we only need to retain the ground state in Eq. (14) and the short time correlations from the static density matrix (2). However, when $t \gtrsim 1/\Delta E$, the full spectrum and excited states of the higher-dimensional parent system become relevant to the subsystem properties, breaking the correspondence to genuinely thermal systems. As a consequence, the entanglement-induced thermal subsystems do not emit thermal radiation, display Johnson-Nyquist noise, or obey fluctuation-dissipation relations. Furthermore, we

cannot expect thermal signatures in any linear-response quantities as they also depend on frequency-resolved correlations (spectral functions of the full system). Thus, in sharp contrast to single-time expectation values, the properties sensitive to temporal correlations behave drastically differently from true thermal systems.

## III. THERMAL SUBSYSTEMS AND THE TABLE OF TOPOLOGICAL INSULATORS

The entanglement-temperature mapping for lower-dimensional subsystems has particularly interesting implications for topological materials. These materials can be arranged into a periodic table in terms of symmetry class and dimensionality, which repeats itself every eight dimensions [33,34]. The topological classes of adjacent dimensionality are connected through Bott periodicity, which maps a topological system in $d$ dimensions to one in $d+1$ dimensions with the same topological invariant by adding or removing chiral symmetry. Typically, this is used to establish connections between different physical systems, e.g., between one-dimensional chains and the scattering invariant of two-dimensional systems [35]. Alternatively, one can introduce additional variables describing synthetic dimensions to carry out quantized pumping, which can also be realized experimentally [36,37].

Since topological phases at different dimensions have Dirac Hamiltonian representatives, we can apply the entanglement-temperature mapping to study them. We show that the reduced density matrices of lower-dimensional subsystems have thermal form with respect to ESHs that exhibit the same topological classification as the table of topological insulators. By carrying out different subsystem measurements, the dimensional reduction actually becomes observable in a single physical system. Furthermore, we illustrate the general pattern of how a hot gapless $D_s$-dimensional subsystem emerges from a $D$-dimensional gapped vacuum state, as pointed out in Sec. II B.

### A. Dimensional reduction from the 4D parent state

To demonstrate the connection between the thermal subsystem entanglement spectra and the dimensional hierarchy of topological materials, we explicitly derive lower-dimensional reduced density matrices of the 4D quantum Hall state [38,39]. This model is widely known as the *parent* Hamiltonian for descendants' topological states using the standard dimensional reduction procedure [33,34,39–41]. The lattice version of this model can be written in the form (1) with a five-component vector

$$\mathbf{d}_{4\mathrm{D}}(\mathbf{k}) = \left(m - \sum_{i=1}^{4} \cos k_i\right)\hat{\mathbf{e}}_0 + \sum_{i=1}^{4} \sin k_i\, \mathbf{e}_i, \tag{15}$$

TABLE I. Dimensional reduction: symmetry classes and phase boundaries of the 4D parent system and lower-dimensional subsystems.

| Dimension | Symmetry class | | Gapless points |
|---|---|---|---|
| 4D | AII | A | $m_c = \pm 4, \pm 2, 0$ |
| 3D | DIII | AIII | $m_c = \pm 3, \pm 1$ |
| 2D | D | A | $m_c = \pm 2, 0$ |
| 1D | BDI | AIII | $m_c = \pm 1$ |
| 0D | AI | A | $m_c = 0$ |

which depends on 4D momentum $\mathbf{k}$. Here, we can introduce a basis where the five $\Gamma$ matrices are given by $\mathbf{\Gamma} = (\tau_z \otimes \sigma_0, \tau_y \otimes \sigma_x, \tau_y \otimes \sigma_y, \tau_y \otimes \sigma_z, \tau_x \otimes \sigma_0)$. The spectrum of the Hamiltonian possesses a pair of twofold degenerate bands with energies $\varepsilon_{\pm}(\mathbf{k}) = \pm|\mathbf{d}(\mathbf{k})|$. Unlike the 2D Chern insulator, which explicitly breaks time-reversal symmetry (TRS), the corresponding 4D model has a time-reversal symmetry $\mathcal{T} H_{4\mathrm{D}}(\mathbf{k}) \mathcal{T}^{-1} = H_{4\mathrm{D}}(-\mathbf{k})$ with time-reversal operator $\mathcal{T} = i\tau_z \otimes \sigma_y \mathcal{K}$ based on the above choice for the $\Gamma$ matrices. Hence, Hamiltonian (15) belongs to the symmetry class AII in the periodic table of the topological insulators. Nonetheless, since the topological classification of 4D topological phases in classes AII and A coincide, we can equally consider the same model as a parent Hamiltonian in class A by adding a small TRS breaking term. Then, according to the Bott periodicity depending on the symmetry class of the parent 4D system, we obtain two different generations of topological phases in lower dimensions belonging to different symmetry classes, as summarized in Table I.

Next, we consider lower-dimensional subsystems of the 4D Hamiltonian (15). According to Eq. (6), for generalized Dirac Hamiltonians (1), the subsystem density matrix is determined by the effective Hamiltonian obtained by averaging the $\mathbf{d}$ vector over the $4 - D_s$ transverse momenta. Thus, the ESH is determined by Eqs. (7) and (8) and given by

$$\mathbf{d}_{D_s} = \left[m - \delta m_{D_s}(\mathbf{k}_{D_s}) - \sum_{i=1}^{d} \cos k_i\right]\hat{\mathbf{e}}_0 + \sum_{i=1}^{d} \sin k_i \hat{\mathbf{e}}_i,$$
$$\delta m_{D_s} = \frac{1}{\mathcal{F}_{D_s}} \int \frac{dk_4 \cdots dk_{D_s+1}}{(2\pi)^{4-D_s}} \frac{\cos k_4 + \cdots + \cos k_{D_s+1}}{|\mathbf{d}_{4\mathrm{D}}|}. \tag{16}$$

The entanglement temperature then follows from Eq. (10). The gapless points of the ESHs, signifying possible topological phase boundaries, are given by the condition $\mathbf{d}_{D_s} = 0$. This can only take place at the high-symmetry points $Q_i$ of the subsystem Brillouin zone, where $\sin Q_i = 0$ for $i = 0, \ldots, d$. Hence, at different $Q$ points, the gap-closing condition becomes $\mathbf{d}_{D_s}(\mathbf{Q}) = [m - \delta m_{D_s}(\mathbf{Q}) - \sum_{i=1}^{d} \cos Q_i]\hat{\mathbf{e}}_0 \equiv 0$. Since the shifts in the mass vanish at

high-symmetry points [$\delta m_{D_s}(\mathbf{Q}) = 0$] implied by Eq. (16), the critical values are then given by $m_c = \sum_{i=1}^{d} \cos Q_i$.

All of the descendent models as well as the parent systems have a $\mathbb{Z}$-classified topology that is characterized by Chern and winding numbers in even and odd dimensions, respectively. This property holds irrespective of whether one regards the 4D parent state as belonging to class A or AII. For a Hamiltonian given in terms of $n+1$ different anticommuting Dirac matrices and in $n$ spatial dimensions, the $\mathbb{Z}$ invariant has a generic form

$$\nu_n = \frac{1}{S_n} \int d^n k \epsilon^{\mu_0 \cdots \mu_n} \hat{d}_{\mu_0} (\partial_{k_1} \hat{d}_{\mu_1}) \cdots (\partial_{k_n} \hat{d}_{\mu_n}),$$

in terms of the mapping $\hat{\mathbf{d}}(\mathbf{k}) = \mathbf{d}(\mathbf{k})/|\mathbf{d}(\mathbf{k})|$ from the $n$-dimensional Brillouin zone to the $n$-dimensional unit sphere [42]. The prefactor $S_n = 2\pi^{(n+1)/2}/\Gamma[(n+1)/2]$ given in terms of the gamma function denotes the area of the $n$-dimensional unit sphere. The topological invariant for the 4D parent Hamiltonian and the lower-dimensional entanglement Hamiltonians can be evaluated straightforwardly and the results are summarized in Fig. 4. We observe that the topological invariant always changes at each gapless point and then identically vanishes for $|m| > d$ (where $1 \leq d \leq 4$), indicating a trivial topological phase. In particular, we find that the ESHs have distinct topological landscapes with phase boundaries that move with the subsystem dimension $d$. Although this conclusion relies on the specific model (15), the gap-closing pattern of the lower-dimensional ESHs is more general, as discussed in Appendix A. At the critical point of the subsystem, the spectrum of the ESH actually describes a semimetal at finite temperature. This systematizes the observation in Sec. II B that the lower-dimensional subsystems of a gapped system at zero temperature may actually appear as a metallic state at finite temperature. It also offers an intuitive explanation for the emergence of the gapless subsystems as follows. We have demonstrated that the process of tracing out the higher-dimensional complement to obtain the lower-dimensional ESH has analogous features with the usual process of dimensional reduction. In this process, the system parameters controlling the gap closings of lower-dimensional systems are generically renormalized. Likewise, the renormalization of parameters in the ESH, which is ultimately responsible for the emergence of hot gapless subsystems of zero-temperature insulators, can be regarded as a reflection of what is expected from the conventional dimensional reduction. This argument applies to the generic spatial dimension and also suggests that it is largely insensitive to the details of the considered model. Therefore, from a physical point of view, the emergence of hot metallic subsystems from vacuum fluctuations of gapped systems is not limited to a specific model, which makes it even more remarkable.

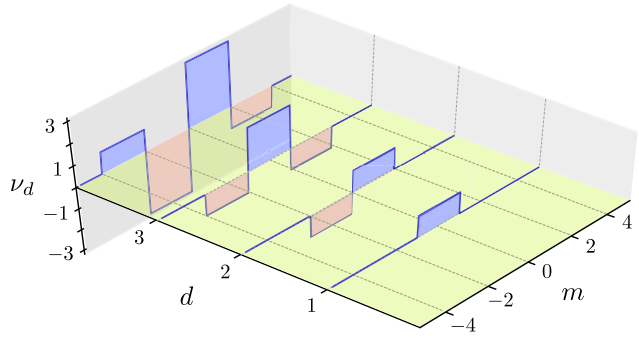


FIG. 4. Topological invariant $\nu_d$ of the 4D quantum Hall model and its lower-dimensional effective subsystem Hamiltonians as a function of the band mass $m$.

Finally, we note that the symmetries of the dimensional-reduced entanglement Hamiltonians are in agreement with the Bott periodicity of topological insulators. As can be seen in Eq. (16), the $d$-dimensional entanglement Hamiltonian depends only on the first $d+1$ Dirac matrices. As a consequence, the 3D subsystem not only inherits the TRS from the parent 4D Hamiltonian, but also acquires a particle-hole symmetry (PHS) as $\mathcal{P} H_{3D}(\mathbf{k}) \mathcal{P}^{-1} = -H_{3D}(\mathbf{k})$ with $\mathcal{P} = \tau_y \otimes \sigma_y \mathcal{K}$. The presence of both TRS and PHS induce chiral symmetry $\mathcal{C} = \mathcal{P}\mathcal{T} = \tau_x \otimes \sigma_0$, indicating that the 3D model belongs to the class DIII. With similar reasoning, one can figure out the symmetry classes of the lower-dimensional descendants as listed in Table I. Thus, the entanglement-temperature mapping reflects the periodic table of topological insulators. In Appendix B, we discuss how the reduced density matrix also reflects the topological properties of weak topological insulators.

## IV. EXPERIMENTAL CONSEQUENCES

The emergence of thermal states from the ground-state entanglement reflects the highly nontrivial nature of the quantum vacuum. Although two special cases of this phenomenon, the Hawking and Unruh effects, have been known for half a century, the phenomenon has eluded experimental confirmation. The first experimental observation of thermal states from vacuum entanglement would be an outstanding achievement, bridging fundamental notions of quantum information, statistical physics, condensed-matter physics, and high-energy physics. Here we propose a concrete setup to observe the vacuum thermalization within currently existing technology. The most natural setting for exploring our findings is ultracold atoms in optical lattices. Such systems are considered ideal for quantum simulation for a wide variety of quantum phenomena due to their high level of control and accuracy [43–46]. Moreover, it has been previously established that these systems can realize various topological systems [47–49]. In particular, the Haldane model [47] can be represented as a

massive two-band Dirac Hamiltonian (1) and is directly relevant for our discussion. Moreover, the QWZ model studied in Sec. II B has already been realized in bosonic systems [50,51]. Thus, two-band Dirac systems are suitable candidates for experimental studies.

The entanglement-induced thermalization in these systems could be probed by comparing the entanglement-governed fluctuations in subsystems with genuinely thermal fluctuations. This idea had been previously used to introduce an effective temperature for subsystems of a 1D spin system [52]. But, as we have thoroughly discussed in Sec. II D, for such situations, a unique unambiguous definition of entanglement temperature is almost impossible due to its position dependence. Nevertheless, using the fluctuations, it has been found that the effective temperature of a subsystem vanishes as $T_{\text{eff}} \propto \log L/L$ for large subsystem sizes [53]. In sharp contrast, for lower-dimensional subsystems, we see that the entanglement temperature is enormous as it scales with the lateral hopping term and can be much higher than the real temperature in the experiment. As long as the real temperature is low compared to the hopping amplitudes, it has little effect on the outcome of the experiment. Moreover, the effective entanglement temperature can be easily controlled by varying the hopping amplitude out of the subsystem. Fluctuations of the subsystem observables match those of thermal systems at corresponding temperature, thus providing a feasible experimental signature to probe the entanglement-induced thermalization.

We illustrate the above recipe by studying the behavior of particle fluctuations in a 1D subsystem of the QWZ model studied in Sec. II B. The subsystem particle number operator is defined as $\hat{N} = \sum_i \hat{c}_i^\dagger \hat{c}_i$, where the summation is restricted to a chain in the $x$ direction embedded in the 2D lattice. The subsystem particle number fluctuations are quantified by their variance $\Delta N^2 = \langle \hat{N}^2 \rangle - \langle \hat{N} \rangle^2$. We consider two different values for the lateral hopping, $t_y/t_x = 1$ and $t_y/t_x = 0.5$, which translate to different effective temperatures. The corresponding correlation matrix spectra (or population probabilities) of the 1D subsystem are shown in Figs. 5(a) and 5(b). As seen in Figs. 5(c) and 5(d), the comparison of the particle fluctuations as a function of the mass parameter in the subsystem with that of the associated 1D system at a constant temperature shows excellent agreement. When the effective temperature is reduced by decreasing the lateral hopping to $t_y/t_x = 0.5$, the gap-closing points of the ESH (and the correlation spectrum) at $m = \pm 1$ become clearly visible through enhanced fluctuations signaled by the two peaks. The positions of these peaks, obscured by high effective temperature at $t_y/t_x = 1$, do not coincide with the 2D gap-closing points ($|m| = 2$, $m = 0$) but provide a smoking gun signature of our prediction that a 1D subsystem in the gapped 2D subsystem at zero temperature can appear as a hot gapless subsystem. Moreover, the fluctuations of conserved quantities can be exploited as an effective measure of entanglement entropy. The connection linking fluctuations and entanglement entropy, which was previously considered in various studies, especially in a transport context [54–56], has been put in a general framework by justifying the similarities between entanglement entropy and variance of conserved subsystem observables [57]. Thus, the agreement between the fluctuations, as shown in Fig. 5, implies that the entanglement entropy of the 1D subsystem corresponds to the thermodynamic entropy of a genuine 1D system at a constant temperature.

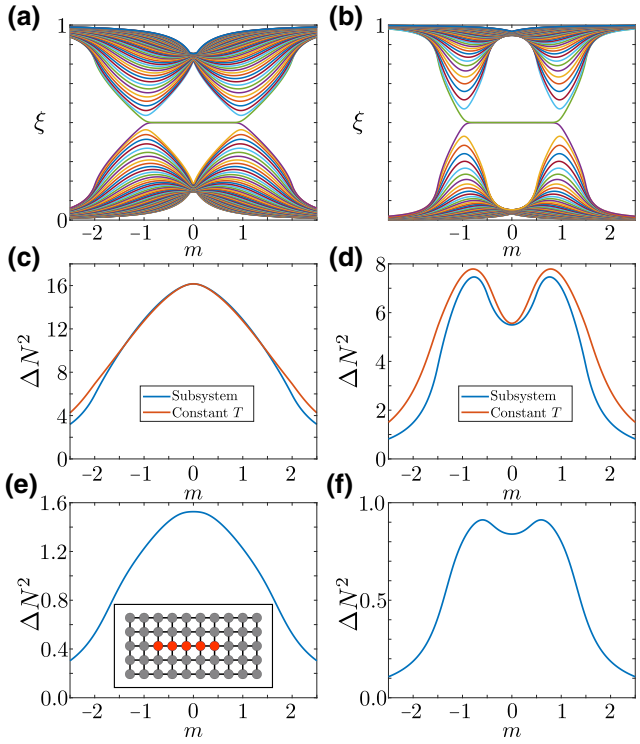


FIG. 5. Correlation matrix spectra and particle number variances of finite 1D subsystems of a 2D QWZ model, with different orthogonal hoppings corresponding to different effective temperatures in the mapping to 1D systems. The red curve in the bottom figures also shows the fluctuations obtained using Eq. (11), but with a constant temperature simply equal to the mean over $k$ of the temperature given by Eq. (10) [with the $k$-dependent $T(k)$, the fluctuations would match exactly]. (a),(c) All hoppings of equal magnitude. (b),(d) Orthogonal hoppings half the magnitude of hoppings parallel to the chain, corresponding to a lower effective temperature. (e) Particle number variance of a subsystem of length 5 in a total system of size $5 \times 10$ with open boundary conditions. Inset: schematic illustration of the system. (f) Same as (e), but with $y$-directional hoppings half the magnitude of those in the $x$ direction.

Importantly, the qualitative behavior of the fluctuations is preserved even at small system sizes accessible in current experiments. This is illustrated in Figs. 5(e) and 5(f), where we show $\Delta N^2$ for a subsystem of length 5 embedded in a $5 \times 10$ array. Manipulating comparable lattice sizes are within reach of the current experimental techniques

[58–60]. Moreover, a site-resolved measurement of particle number statistics, similar to what is needed in our proposal, has already been demonstrated in Refs. [43,44]. Thus, the thermal state arising from ground-state entanglement could be observed by realizing a two-band Dirac insulator and carrying out a site-resolved particle number measurement, both of which have been previously demonstrated in cold-atom experiments.

Finally, we emphasize the sharp distinction between our experimental proposal and a number of recent works with superficial similarities. First, the recent experiments simulating some aspects of the Hawking and Unruh effects [61–63], unlike in our proposal, apply time-dependent driving to stimulate a thermal-like radiation in systems that are not described by a static thermal density matrix. In this sense, they do not constitute a demonstration of thermal states emerging from vacuum entanglement. Similarly, the purpose and the outcome of previous works simulating entanglement Hamiltonians [27,28,64] are equally distinct from our theoretical proposal. The main purpose of these works is to artificially realize entanglement Hamiltonians for certain lattice models that follow, at least approximately, the BW ansatz. As has been thoroughly discussed in Sec. II D, the artificial simulation of entanglement Hamiltonians, while interesting in its own right, cannot be regarded as a confirmation of vacuum-entanglement-induced thermalization, and nor do the cited works claim so. In our experimental scheme, we suggest to directly observe the subsystem particle number fluctuations that follow a thermal equilibrium form, thus directly revealing the thermal nature of the reduced system. In this definite sense, our proposal would indeed enable the first observation of vacuum-entanglement-induced effective temperature.

## V. CONCLUSION

In this work we identified a large class of quantum many-body systems, constituting of gapped Dirac fermions, in which entanglement of vacuum fluctuations gives rise to a thermal density matrix in their lower-dimensional subsystems. We also showed that, remarkably, subsystems of a zero-temperature insulator may even appear as hot gapless systems. We proposed that the emergence of a thermal state from vacuum could be realistically observed, for the first time, in cold-atom quantum simulators through thermal fluctuations. Direct experimental verification of an emergent thermal state from vacuum quantum fluctuations would be an outstanding achievement with ramifications in statistical physics, condensed-matter physics, high-energy physics, and quantum information.

## ACKNOWLEDGMENTS

The authors acknowledge the Academy of Finland project 331094 for support.

## APPENDIX A: GAP CLOSING IN DIMENSIONALLY REDUCED SYSTEMS

Let us assume that we have a Dirac-type Hamiltonian

$$H_k = \sum_{i=1}^{N} d_i(\mathbf{k})\Gamma_i, \tag{A1}$$

where the $\Gamma_i$ are $2^n \times 2^n$ general gamma matrices that obey the anticommutation rule $\{\Gamma_i, \Gamma_j\} = 2\delta_{ij}$.

Let us assume that the system is $D$ dimensional and translationally invariant, and that the subsystem considered for the $\mathcal{C}$ matrix is $(D-1)$ dimensional and likewise translationally invariant. As mentioned in the main text, the $\mathcal{C}$ matrix at $T = 0$ can then be written as

$$\mathcal{C}(k_\parallel) = \frac{1}{L} \sum_{\text{filled } \nu, k_\perp} |\psi_{\nu,\mathbf{k}}\rangle\langle\psi_{\nu,\mathbf{k}}|. \tag{A2}$$

In the above we have written $\mathbf{k} = (k_\parallel, k_\perp)$, where $k_\parallel$ are the momenta inside the subsystem and $k_\perp$ represents the single momentum component orthogonal to the subsystem. Because of the structure of the Hamiltonian, the above is equivalent to

$$\mathcal{C}(\mathbf{k}_\parallel) = \mathbb{1} - \frac{1}{L} \sum_{k_\perp, i} \frac{d_i(\mathbf{k})}{d(\mathbf{k})}\Gamma_i \equiv \mathbb{1} - B(\mathbf{k}_\parallel). \tag{A3}$$

A gap closing corresponds to $B$ having zero-energy eigenvalues for some $\mathbf{k}_\parallel$. Let us now separate the part of the Hamiltonian that depends on the orthogonal momentum, i.e.,

$$d_i(\mathbf{k}) = h_i(k_\parallel) + f_i(k_\parallel, \mathbf{k}_\perp). \tag{A4}$$

In this way we have separated a lower-dimensional Hamiltonian expressed in terms of $h_i$:

$$H_{D-1}(\mathbf{k}_\parallel) = \sum_{i=1}^{N} h_i(\mathbf{k}_\parallel)\Gamma_i. \tag{A5}$$

The functions $f$ may or may not be $\mathbf{k}_\parallel$ dependent (as, e.g., would occur with diagonal hoppings).

Let us now consider a momentum $\mathbf{k}_\parallel = \mathbf{q}_0$ where $H_{D-1}$ has a gap closing, so that, for all $i$, $h_i(\mathbf{q}_0) = 0$. At this particular point, the $\Gamma$ components of $B$ take the form

$$B(\mathbf{q}_0)_i = \frac{1}{L} \sum_{k_\perp} \frac{f_i(k_\perp, \mathbf{q}_0)}{\sqrt{\sum_j f_j(k_\perp, \mathbf{q}_0)^2}}. \tag{A6}$$

Let us first assume that, for every $i$, the function $f_i(k_N, \mathbf{q}_0)$ is either even or odd around $k_\perp = 0$ (note that this does not

need to be the case for a generic $\mathbf{k}_\parallel$). In this case, where it is odd, $B_i$ vanishes, and where it is even, it reduces to

$$B(\mathbf{q}_0)_i = 2\frac{1}{L_N}\sum_{k_D<\pi}\frac{f_i(k_\perp,\mathbf{q}_0)}{\sqrt{\sum_j f_j(k_\perp,\mathbf{q}_0)^2}}. \quad \text{(A7)}$$

If now within this $k_\perp$ interval the numerator is odd and the denominator even around $\pi/2$, the whole sum vanishes. This will occur if, for every $i$, and $0 \le \epsilon \le \pi/2$, $|f_i(\pi/2+\epsilon,\mathbf{q}_0)| = |f_i(\pi/2-\epsilon,\mathbf{q}_0)|$, and further $f_i(\pi/2+\epsilon,\mathbf{q}_0) = -f_i(\pi/2-\epsilon,\mathbf{q}_0)$ for those $i$ for which $f_i(k_\perp,\mathbf{q}_0)$ is even around $k_\perp = 0$. This will be the case, e.g., for nearest-neighbour hopping on a lattice. If so, gap closings of $H_{D-1}$ immediately imply gap closings of $H_k$.

## APPENDIX B: THERMAL LOWER-DIMENSIONAL SUBSYSTEMS IN WEAK TOPOLOGICAL INSULATORS

Here we show how the lower-dimensional thermal subsystems reflect the topological properties of weak topological insulators. One way to construct a model for a 2D weak topological insulator (WTI) is to consider a vertical stack of Su–Schrieffer–Heeger chains with nearest-neighbor unit cells coupled in the vertical direction as shown in the inset of Fig. 6. The two-band Hamiltonian of the model can be written in the Dirac form $H_{2D} = \mathbf{d}_{\mathrm{WTI}}(\mathbf{k})\cdot\boldsymbol{\sigma}$ with

$$\mathbf{d}_{\mathrm{WTI}}(\mathbf{k}) = (t_x + t_x'\cos k_x + 2t_y\cos k_y, t_x'\sin k_x, 0). \quad \text{(B1)}$$

This Hamiltonian clearly satisfies the chiral symmetry as we have $\sigma_z H \sigma_z = -H$. Hence, the topological characterization of the model is encoded in the weak indices $\nu_j = -i\int d^2\mathbf{k}/(2\pi)^2\, Q_{\mathbf{k}}^{-1}\partial_{k_j} Q_{\mathbf{k}}$, which are based on the vertical averaging over the 1D winding number densities. Here, $Q_{\mathbf{k}} = d_x + id_y$, where $d_x$, $d_y$ denote the components of Eq. (B1). Assuming that $t_y > 0$, the phase diagram of this model consists of a WTI with $(\nu_x,\nu_y) = (1,0)$ for $t_x' - t_x > 2t_y$, a trivial phase for $t_x - t_x' > 2t_y$, and a gapless (metallic) phase for $|t_x' - t_x| < 2t_y$.

In the WTI phase, depending on the orientation of the reduced 1D subsystem with respect to the $x$ and $y$ directions, the entanglement Hamiltonian is in the topological and trivial phases, respectively. This distinction, which reflects the weak topological index of the parent 2D system, is illustrated in Fig. 6. The topology of the 1D ESH is easily obtained from the $\mathbf{d}$ vectors of the subsystems along the $x$ and $y$ directions,

$$d_{1x}(k) = [t_x + t_x'\cos k + \delta_x t(k), t_x'\sin k, 0], \quad \text{(B2)}$$

$$d_{1y}(k) = [t_x + 2t_y\cos k + \delta_y t(k), 0, 0], \quad \text{(B3)}$$

which are obtained from Eqs. (7) and (8) by setting $\mathbf{k}_\perp = k_y, k_x$. This elucidates why the ESH for the subsystem

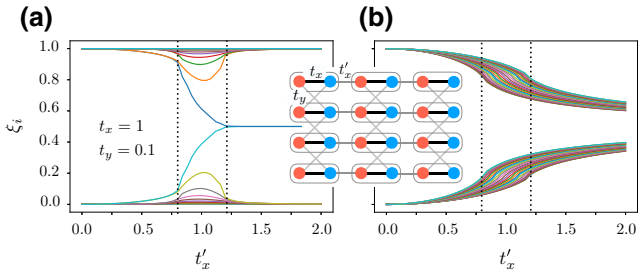


FIG. 6. Correlation matrix spectra for 1D subsystems of the 2D WTI. The system size (number of unit cells) is $60 \times 60$ and the 1D sublattices have length $L = 30$. Panels (a) and (b) indicate the spectra for a 1D open subsystem along $x$ and $y$, respectively. The dotted vertical lines are visual guides for separating different phases, i.e., trivial, gapless, and WTI, respectively.

along $y$ cannot have a topological phase since its winding number vanishes identically. In contrast, $d_{1x}(k)$ for the subsystem along the $x$ axis supports a finite winding number in the same regime as parent Hamiltonian (B1).


[1] Mehran Kardar, *Statistical Physics of Particles* (Cambridge University Press, Cambridge, England, 2007).
[2] J. M. Deutsch, Quantum statistical mechanics in a closed system, Phys. Rev. A **43**, 2046 (1991).
[3] Mark Srednicki, Chaos and quantum thermalization, Phys. Rev. E **50**, 888 (1994).
[4] Marcos Rigol and Mark Srednicki, Alternatives to Eigenstate Thermalization, Phys. Rev. Lett. **108**, 110601 (2012).
[5] Marcos Rigol, Vanja Dunjko, and Maxim Olshanii, Thermalization and its mechanism for generic isolated quantum systems, Nature **452**, 854 (2008).
[6] James R. Garrison and Tarun Grover, Does a Single Eigenstate Encode the Full Hamiltonian?, Phys. Rev. X **8**, 021026 (2018).
[7] Luca D'Alessio, Yariv Kafri, Anatoli Polkovnikov, and Marcos Rigol, From quantum chaos and eigenstate thermalization to statistical mechanics and thermodynamics, Adv. Phys. **65**, 239 (2016).
[8] Joshua M Deutsch, Eigenstate thermalization hypothesis, Rep. Prog. Phys. **81**, 082001 (2018).
[9] Giulio Biroli, Corinna Kollath, and Andreas M. Läuchli, Effect of Rare Fluctuations on the Thermalization of Isolated Quantum Systems, Phys. Rev. Lett. **105**, 250401 (2010).
[10] Luca Bombelli, Rabinder K. Koul, Joohan Lee, and Rafael D. Sorkin, Quantum source of entropy for black holes, Phys. Rev. D **34**, 373 (1986).
[11] Mark Srednicki, Entropy and Area, Phys. Rev. Lett. **71**, 666 (1993).
[12] V. P. Frolov and D. V. Fursaev, Thermal fields, entropy and black holes, Class Quantum Gravity **15**, 2041 (1998).
[13] Sergey N Solodukhin, Entanglement entropy of black holes, Living Rev. Relativity **14**, 8 (2011).

[14] Shinsei Ryu and Tadashi Takayanagi, Aspects of holographic entanglement entropy, J. High Energy Phys. **2006**, 045 (2006).

[15] H. Casini and M. Huerta, Entanglement entropy in free quantum field theory, J. Phys. A **42**, 504007 (2009).

[16] Andreas Osterloh, Luigi Amico, Giuseppe Falci, and Rosario Fazio, Scaling of entanglement close to a quantum phase transition, Nature **416**, 608 (2002).

[17] G. Vidal, J. I. Latorre, E. Rico, and A. Kitaev, Entanglement in Quantum Critical Phenomena, Phys. Rev. Lett. **90**, 227902 (2003).

[18] Pasquale Calabrese and John Cardy, Entanglement entropy and quantum field theory, J. Stat. Mech.: Theory Exp. **2004**, P06002 (2004).

[19] Barbara M. Terhal, Michael M. Wolf, and Andrew C. Doherty, Quantum entanglement: A modern perspective, Phys. Today **56**, 46 (2003).

[20] Luigi Amico, Rosario Fazio, Andreas Osterloh, and Vlatko Vedral, Entanglement in many-body systems, Rev. Mod. Phys. **80**, 517 (2008).

[21] Ryszard Horodecki, Paweł Horodecki, Michał Horodecki, and Karol Horodecki, Quantum entanglement, Rev. Mod. Phys. **81**, 865 (2009).

[22] J. Eisert, M. Cramer, and M. B. Plenio, Colloquium: Area laws for the entanglement entropy, Rev. Mod. Phys. **82**, 277 (2010).

[23] Matthew B. Hastings, An area law for one-dimensional quantum systems, J. Stat. Mech.: Theory Exp. **2007**, P08024 (2007).

[24] M. B. Plenio, J. Eisert, J. Dreißig, and M. Cramer, Entropy, Entanglement, and Area: Analytical Results for Harmonic Lattice Systems, Phys. Rev. Lett. **94**, 060503 (2005).

[25] Joseph J. Bisognano and Eyvind H. Wichmann, On the duality condition for a Hermitian scalar field, J. Math. Phys. **16**, 985 (1975).

[26] Brian Swingle and John McGreevy, Area law for gapless states from local entanglement thermodynamics, Phys. Rev. B **93**, 205120 (2016).

[27] Marcello Dalmonte, Benoît Vermersch, and Peter Zoller, Quantum simulation and spectroscopy of entanglement Hamiltonians, Nat. Phys. **14**, 827 (2018).

[28] M. Dalmonte, V. Eisler, M. Falconi, and B. Vermersch, Entanglement Hamiltonians: from field theory, to lattice models and experiments, (2022), ArXiv:2202.05045.

[29] Mahdieh Pourjafarabadi, Hanieh Najafzadeh, Mohammad-Sadegh Vaezi, and Abolhassan Vaezi, Entanglement Hamiltonian of interacting systems: Local temperature approximation and beyond, Phys. Rev. Res. **3**, 013217 (2021).

[30] Marcos Rigol, Vanja Dunjko, Vladimir Yurovsky, and Maxim Olshanii, Relaxation in a Completely Integrable Many-Body Quantum System: An Ab Initio Study of the Dynamics of the Highly Excited States of 1D Lattice Hard-Core Bosons, Phys. Rev. Lett. **98**, 050405 (2007).

[31] Ingo Peschel, Calculation of reduced density matrices from correlation functions, J. Phys. A **36**, L205 (2003).

[32] Ingo Peschel and Viktor Eisler, Reduced density matrices and entanglement entropy in free lattice models, J. Phys. A: Math. Theor. **42**, 504003 (2009).

[33] Andreas P. Schnyder, Shinsei Ryu, Akira Furusaki, and Andreas W. W. Ludwig, Classification of topological insulators and superconductors in three spatial dimensions, Phys. Rev. B **78**, 195125 (2008).

[34] Alexei Kitaev, Periodic table for topological insulators and superconductors, AIP Conf. Proc. **1134**, 22 (2009).

[35] I. C. Fulga, F. Hassler, and A. R. Akhmerov, Scattering theory of topological insulators and superconductors, Phys. Rev. B **85**, 165409 (2012).

[36] Oded Zilberberg, Sheng Huang, Jonathan Guglielmon, Mohan Wang, Kevin P. Chen, Yaacov E. Kraus, and Mikael C. Rechtsman, Photonic topological boundary pumping as a probe of 4D quantum Hall physics, Nature **553**, 59 (2018).

[37] Michael Lohse, Christian Schweizer, Hannah M. Price, Oded Zilberberg, and Immanuel Bloch, Exploring 4D quantum Hall physics with a 2D topological charge pump, Nature **553**, 55 (2018).

[38] Shou-Cheng Zhang and Jiangping Hu, A four-dimensional generalization of the quantum Hall effect, Science **294**, 823 (2001).

[39] Xiao-Liang Qi, Taylor L. Hughes, and Shou-Cheng Zhang, Topological field theory of time-reversal invariant insulators, Phys. Rev. B **78**, 195424 (2008).

[40] Xiao-Liang Qi and Shou-Cheng Zhang, Topological insulators and superconductors, Rev. Mod. Phys. **83**, 1057 (2011).

[41] Ching-Kai Chiu, Jeffrey C. Y. Teo, Andreas P. Schnyder, and Shinsei Ryu, Classification of topological quantum matter with symmetries, Rev. Mod. Phys. **88**, 035005 (2016).

[42] The invariant given in terms of the map $\hat{\mathbf{d}}_{\mathbf{k}}$ has a simple geometric meaning as the number of times the unit vector $\hat{\mathbf{d}}_{\mathbf{k}}$ wraps around the $n$-sphere when $\mathbf{k}$ sweeps the whole Brillouin zone. Such a intuitive interpretation of the topological invariant translates to the more rigorous understanding that the $n$th homotopy class of the $n$ sphere is equivalent to $\mathbb{Z}$: $\pi_n(S^n) \equiv \mathbb{Z}$.

[43] Adam M. Kaufman, M. Eric Tai, Alexander Lukin, Matthew Rispoli, Robert Schittko, Philipp M Preiss, and Markus Greiner, Quantum thermalization through entanglement in an isolated many-body system, Science **353**, 794 (2016).

[44] Rajibul Islam, Ruichao Ma, Philipp M. Preiss, M. Eric Tai, Alexander Lukin, Matthew Rispoli, and Markus Greiner, Measuring entanglement entropy in a quantum many-body system, Nature **528**, 77 (2015).

[45] Christian Gross and Immanuel Bloch, Quantum simulations with ultracold atoms in optical lattices, Science **357**, 995 (2017).

[46] Tiff Brydges, Andreas Elben, Petar Jurcevic, Benoît Vermersch, Christine Maier, Ben P. Lanyon, Peter Zoller, Rainer Blatt, and Christian F. Roos, Probing Rényi entanglement entropy via randomized measurements, Science **364**, 260 (2019).

[47] Gregor Jotzu, Michael Messer, Rémi Desbuquois, Martin Lebrat, Thomas Uehlinger, Daniel Greif, and Tilman Esslinger, Experimental realization of the topological Haldane model with ultracold fermions, Nature **515**, 237 (2014).

[48] Monika Aidelsburger, Michael Lohse, Christian Schweizer, Marcos Atala, Julio T. Barreiro, Sylvain Nascimbène, N. R. Cooper, Immanuel Bloch, and Nathan Goldman, Measuring the Chern number of Hofstadter bands with ultracold bosonic atoms, Nat. Phys. **11**, 162 (2015).

[49] Nathan Goldman, Jan C Budich, and Peter Zoller, Topological quantum matter with ultracold gases in optical lattices, Nat. Phys. **12**, 639 (2016).

[50] Zhan Wu, Long Zhang, Wei Sun, Xiao-Tian Xu, Bao-Zong Wang, Si-Cong Ji, Youjin Deng, Shuai Chen, Xiong-Jun Liu, and Jian-Wei Pan, Realization of two-dimensional spin-orbit coupling for Bose-Einstein condensates, Science **354**, 83 (2016).

[51] N. R. Cooper, J. Dalibard, and I. B. Spielman, Topological bands for ultracold atoms, Rev. Mod. Phys. **91**, 015005 (2019).

[52] V. Eisler, Ö. Legeza, and Z. Rácz, Fluctuations in subsystems of the zero-temperature *XX* chain: Emergence of an effective temperature, J. Stat. Mech.: Theory Exp. **2006**, P11013 (2006).

[53] This result reflects another problem with defining entanglement temperature for subsystems with the same dimensionality as the system, because the resulting average temperature vanishes for very large sizes.

[54] Israel Klich and Leonid Levitov, Quantum Noise as an Entanglement Meter, Phys. Rev. Lett. **102**, 100502 (2009).

[55] H. Francis Song, Stephan Rachel, and Karyn Le Hur, General relation between entanglement and fluctuations in one dimension, Phys. Rev. B **82**, 012405 (2010).

[56] H. Francis Song, Stephan Rachel, Christian Flindt, Israel Klich, Nicolas Laflorencie, and Karyn Le Hur, Bipartite fluctuations as a probe of many-body entanglement, Phys. Rev. B **85**, 035409 (2012).

[57] Kim Pöyhönen, Ali G. Moghaddam, and Teemu Ojanen, Many-body entanglement and topology from uncertainties and measurement-induced modes, Phys. Rev. Res. **4**, 023200 (2022).

[58] Hannes Bernien, Sylvain Schwartz, Alexander Keesling, Harry Levine, Ahmed Omran, Hannes Pichler, Soonwon Choi, Alexander S. Zibrov, Manuel Endres, Markus Greiner, *et al.*, Probing many-body dynamics on a 51-atom quantum simulator, Nature **551**, 579 (2017).

[59] Jiehang Zhang, Guido Pagano, Paul W. Hess, Antonis Kyprianidis, Patrick Becker, Harvey Kaplan, Alexey V. Gorshkov, Z.-X. Gong, and Christopher Monroe, Observation of a many-body dynamical phase transition with a 53-qubit quantum simulator, Nature **551**, 601 (2017).

[60] Sepehr Ebadi, Tout T. Wang, Harry Levine, Alexander Keesling, Giulia Semeghini, Ahmed Omran, Dolev Bluvstein, Rhine Samajdar, Hannes Pichler, Wen Wei Ho, *et al.*, Quantum phases of matter on a 256-atom programmable quantum simulator, Nature **595**, 227 (2021).

[61] Jeff Steinhauer, Observation of quantum Hawking radiation and its entanglement in an analogue black hole, Nat. Phys. **12**, 959 (2016).

[62] Juan Ramón Muñoz de Nova, Katrine Golubkov, Victor I. Kolobov, and Jeff Steinhauer, Observation of thermal Hawking radiation and its temperature in an analogue black hole, Nature **569**, 688 (2019).

[63] Jiazhong Hu, Lei Feng, Zhendong Zhang, and Cheng Chin, Quantum simulation of Unruh radiation, Nat. Phys. **15**, 785 (2019).

[64] Christian Kokail, Bhuvanesh Sundar, Torsten V. Zache, Andreas Elben, Benoît Vermersch, Marcello Dalmonte, Rick van Bijnen, and Peter Zoller, Quantum Variational Learning of the Entanglement Hamiltonian, Phys. Rev. Lett. **127**, 170501 (2021).